JACS
JOURNAL OF THE AMERICAN CHEMICAL SOCIETY

Article

pubs.acs.org/JACS

X-ray and Neutron Scattering Study of the Formation of Core–Shell-Type Polyoxometalates

Panchao Yin,*[,†] Bin Wu,[‡] Eugene Mamontov,[†] Luke L. Daemen,[†] Yongqiang Cheng,[†] Tao Li,[§] Soenke Seifert,[§] Kunlun Hong,[∥] Peter V. Bonnesen,[∥] Jong Kahk Keum,[∥] and Anibal J. Ramirez-Cuesta[†]

[†]Chemical and Engineering Materials Division, Neutron Sciences Directorate, Oak Ridge National Laboratory, Oak Ridge, Tennessee 37831, United States

[‡]Department of Physics and Astronomy, Joint Institute of Neutron Science, University of Tennessee, Knoxville, Tennessee 37996, United States

[§]X-ray Science Division, Advanced Photon Source, Argonne National Laboratory, Argonne, Illinois 60439, United States

[∥]Center for Nanophase Materials Sciences, Oak Ridge National Laboratory, Oak Ridge, Tennessee 37831, United States

Supporting Information

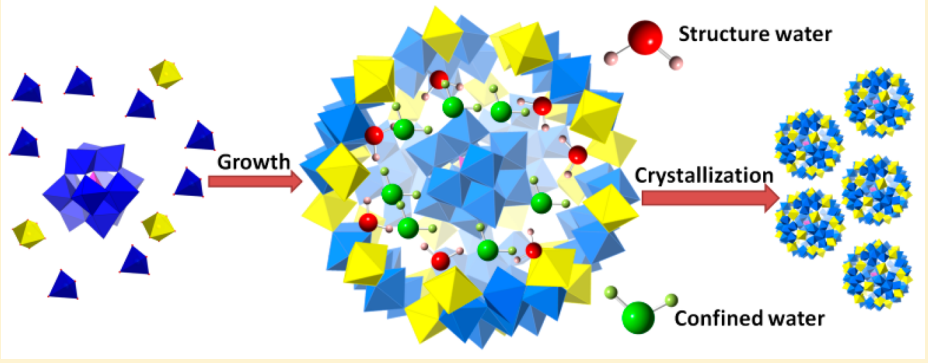

ABSTRACT: A typical type of core–shell polyoxometalates can be obtained through the Keggin-type polyoxometalate-templated growth of a layer of spherical shell structure of $\{Mo_{72}Fe_{30}\}$. Small-angle X-ray scattering is used to study the structural features and stability of the core–shell structures in aqueous solutions. Time-resolved small-angle X-ray scattering is applied to monitor the synthetic reactions, and a three-stage formation mechanism is proposed to describe the synthesis of the core–shell polyoxometalates based on the monitoring results. New protocols have been developed by fitting the X-ray data with custom physical models, which provide more convincing, objective, and completed data interpretation. Quasi-elastic and inelastic neutron scattering are used to probe the dynamics of water molecules in the core–shell structures, and two different types of water molecules, the confined and structured water, are observed. These water molecules play an important role in bridging core and shell structures and stabilizing the cluster structures.

INTRODUCTION

Gigantic polyoxometalates (POMs) are a group of well-defined molecular clusters composed of early transition metal ions and oxo ligands with sizes ranging from ca. 2 to 6 nm.[1−4] Following the seminal work of Müller, gigantic POMs of various sizes and topologies have been obtained, and their molecular structures and applications have been extensively explored.[1−10] In contrast to regular nanoparticles, these POM clusters exhibit well-defined molecular structures (including surface structures) and tunable surface properties, e.g., charge density and hydrophobicity/hydrophilicity.[1−4,11] Therefore, besides their well-developed applications in catalysis and as magnetically/electronically active materials, the gigantic POMs have served as perfect physical models to understand some fundamental science problems, including the solution behavior of polyelectrolytes, interfacial science, and the nature of chirality.[12−19] Moreover, owing to their porous structures and numbers of hydrogen bond donor and acceptor groups on the surface, the clusters have also been widely used in host–guest chemistry and supramolecular science as major building blocks.[20−23] The design and synthesis of gigantic clusters with required shape, size, and surface/electronic properties is critical to extend the applications of the POMs, but the synthetic capability to do this has so far not been attained. Also, additional information will be needed to fully understand the molecular structures and formation mechanism of the gigantic POMs currently in the database.

Recently, mass spectrometry methods have been demonstrated by Cronin to be capable of detecting the intermediate

Received: November 2, 2015
Published: February 5, 2016

DOI: 10.1021/jacs.5b11465
J. Am. Chem. Soc. 2016, 138, 2638–2643

species in the formation process of POMs.[24,25] However, these methods have limited application for gigantic clusters because of the complexity of these systems, resulting from very high molecular weight and large numbers of counter-cations. It is well-known that there could be several species with different arrangements of building blocks that correspond to the same peak in mass spectrum. The lack of morphological information in the mass spectral data makes it difficult to build models to describe the formation process. In the meantime, a few examples have been provided in the existing literature regarding the formation mechanism of POMs. Müller and co-workers have successfully discovered the simultaneous assembly process from $\{Mo_{176}\}$ to $\{Mo_{248}\}$ clusters by studying the structures of single crystals obtained at different synthetic stages.[26] Cronin et al. applied a flow system to investigate the assembly process of small building units into the $\{Mo_{150}\}$ molecular wheel structure.[27] The crystallization of intermediate species unveils that $\{Mo_{36}\}$ clusters serve as templates during the above-mentioned assembly process.[27] However, there are obvious disadvantages to using crystallization in formation mechanism studies: only the robust molecular clusters, which can survive during the crystallization process, can be observed and reported. Therefore, information on the clusters formed in solution is missed because: (1) not all of the clusters can be crystallized and (2) the clusters might decompose/transform to form other species during the crystallization process.

X-ray and neutron scattering techniques are highly suitable for probing topological and dynamics information on POMs with high sensitivity and resolution. Due to the nature of their interaction with matter, X-ray and neutron scattering are sensitive to the heavy metal ions and the hydrogen-enriched water/organic molecules, respectively.[28] The combination of these techniques can provide full information on structure features of POM clusters. Due to its appropriate spatial range (ca. 1−40 nm) and time resolution (<0.1 s), small-angle X-ray scattering (SAXS), especially synchrotron-based SAXS, is ideal for monitoring the formation process of POM clusters under different synthetic conditions at different time frames.[29−38] In the previous literature, the radius of gyration (R_g) and the distance distribution function ($p(r)$) were reported for analysis of the SAXS monitoring data.[29−38] The R_g values were deduced from the SAXS data via Guinier plot, and $p(r)$ was obtained from indirect Fourier transformation.[30,39,40] The accurate acquisition of R_g and $p(r)$ requires the homogeneous and monodisperse nature of reaction solutions.[30,39,40] However, provided the fact that reactants, intermediate species, and products coexist in the reaction solutions, the obtained R_g and $p(r)$ are indeed questionable. Moreover, most of the previous work fails to take into account the effect of structure factor during data analysis.[29−38] Therefore, considering the physics behind Guinier plot and indirect Fourier transformation and the complexity of the reaction solutions, the previous data analysis protocols are not appropriate for monitoring the reaction solutions. In our manuscript, structural features of reactants and products were first fully explored and then used for describing the formation process of the giant core−shell molecules. Meanwhile, quasi-elastic and inelastic neutron scattering (QENS and INS) measurements can provide information on the dynamics of molecules at a wide range of energy scales.[41] QENS and INS are very unique and effective methods to differentiate between structural and nonstructural water and between nonstructural confined and nonstructural bulklike water populations. Due to its simplicity in both synthesis and molecular structure, the classical core−shell POMs ($Na_6[SiMo^{VI}_{12}O_{40}@Mo^{VI}_{68}Mo^{V}_{4}Fe^{III}_{30}O_{252}(CH_3CO_2)_{16}(H_2O)_{100}]$, abbreviation: Keg@$\{Mo_{72}Fe_{30}\}$) were selected as a model to uncover the possible formation mechanism of spherical POM clusters (Figure 1).[42−45] Herein, we report, to the best of our knowledge, the first combination of SAXS, QENS, and INS studies of the structures and formation mechanism of core−shell POMs.

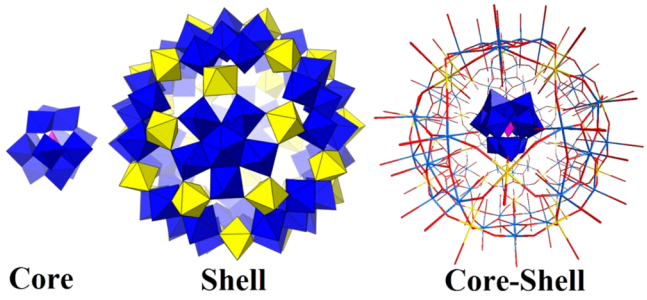

Figure 1. Molecular structures of core, shell, and core−shell structures. Polyhedron code: blue, MoO_6 and MoO_7; yellow, FeO_6; purple, SiO_4. Stick code: blue, Mo; yellow, Fe; red, O.

EXPERIMENTAL SECTION

SAXS Experimental Section. The SAXS experiments were performed at the 12-ID-B and 12-ID-C station with X-ray energy of 12 keV at the Advanced Photon Source of the Argonne National Laboratory. The sample to detector distance was about 2 m. A Pilatus detector (Dectris Ltd.) was used to acquire images with typical exposure times in the range of 0.1−1.0 s for a single measurement. The sample solutions were put in quartz capillaries for all the measurements. For each of the sample measurements, SAXS measurements of corresponding solvents were also carried out for background reduction. The fitting of data from core and shell samples was performed by using Crysol. Structure files in PDB format used in Crysol were transformed from CIFs of the corresponding data under Materials Studio 8.0. The theoretical scattering function from combined core−shell structure with a trial offset is calculated from the following equation

$$I_{th}(q) = A\langle \sum_i \sum_j b_i b_j e^{-i\vec{q}\cdot(\vec{r}_i-\vec{r}_j)}\rangle + B$$

where A and B are scaling factors independent of scattering vector $\vec{q}$. b and r denote the scattering length and position of a particle indexed by subscripts i or j. The summations both run over all the particles from the core−shell structure, while the angular bracket represents the average over the directions of $\vec{q}$.

QENS Experimental Section. The sample was loaded in a flat-plate aluminum sample holder with an active area of 3 cm × 5 cm and then sealed with an indium wire and placed in a closed-cycle refrigerator providing a temperature stability of better than 1 K. The neutron measurements were performed at the SNS backscattering spectrometer, BASIS.[46] The energy resolution measured from the sample cooled to 10 K showed a Q-averaged value of 3.4 μeV (fwhm). The range of energy transfer of ±100 μeV was used for data analysis. The data collected at 300 K and averaged over the momentum transfer range of 0.2 Å^{-1} < Q < 1.2 Å^{-1} were reduced using standard MANTID-based routines and analyzed using the DAVE software package.[47] Besides a sloped background term, the fit function included a delta-fucnction centered at zero energy transfer and a Lorentzian, both convolved with the spectrometer resolution function. The first of these terms is due to the species immobile on the resolution scale of the spectrometer (about 0.4 ns), such as structural water molecules, whereas the second term originates from the localized diffusion of the

DOI: 10.1021/jacs.5b11465
J. Am. Chem. Soc. 2016, 138, 2638−2643

disordered water molecules. The use of the Q-averaged data was dictated by the weak (in comparison with the elastic peak) quasi-elastic component and made possible by the highly localized diffusion dynamics of water molecules, which yields Q-independent broadening of the quasi-elastic signal.

INS Experimental Section. INS measurements of core−shell samples were performed on beamline 16B, the Vibrational Spectrometer (VISION) at SNS, ORNL, Oak Ridge, TN.[48] The powder sample (∼1 g) was loaded into 8 mm diameter vanadium cylindrical canisters sealed with copper gaskets and then cooled to the base temperature (∼5 K). An empty V-canister of the same type was measured for background subtraction. The measurements were carried out at 10, 50, 100, 150, and 200 K, respectively.

RESULTS AND DISCUSSIONS

SAXS studies are applied to explore the structures and stability of core−shell POMs in solution. The synthesis of Keg@{$Mo_{72}Fe_{30}$} and similar compounds is well-developed and described in the previous literature.[42−45] The freshly prepared core−shell samples are still soluble in water, whereas the dissolution process would be difficult once the samples are air-dried and cross-linked. SAXS studies at room temperature on the aqueous solutions of the core ($H_4SiMo_{12}O_{40}$, Keg), the shell ($[Mo_{72}Fe_{30}O_{252}(CH_3COO)_{12}\{Mo_2O_7(H_2O)\}_2\{H_2Mo_2O_8(H_2O)\}(H_2O)_{91}]\cdot\sim150H_2O$, $\{Mo_{72}Fe_{30}\}$), and the core−shell (Keg@$\{Mo_{72}Fe_{30}\}$) samples with concentration at 1 mg/mL indicate their unique structural features and stability in solutions (Figures 1 and 2). The core−shell and shell

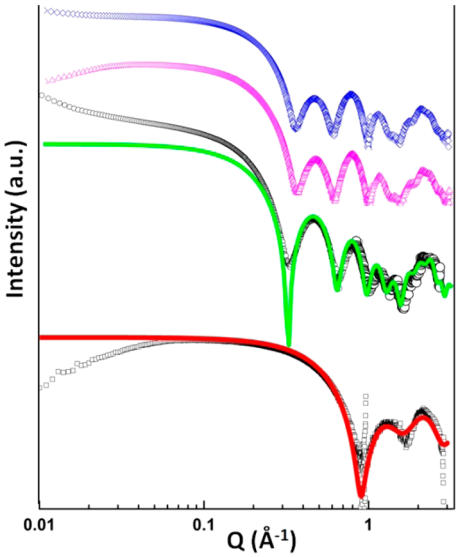

Figure 2. Experimental SAXS data of the aqueous solutions of Keg (black square), $\{Mo_{72}Fe_{30}\}$ (black circle), and Keg@$\{Mo_{72}Fe_{30}\}$ (freshly prepared, purple triangle; two-week aged, blue diamond) and the fitting curves generated by Crysol from the single-crystal data of Keg (red) and $\{Mo_{72}Fe_{30}\}$ (green).

compounds show similar scattering curves because of their identical size and similar spherical structural features, which are obviously different from those of the core sample. A detailed analysis of the SAXS data for the core−shell sample indicates that the first minimum point (from left to right) of the core−shell sample shifts from 0.316 to 0.339 $Å^{-1}$, and the intensity ratio of the first two oscillation peaks (I_1/I_2) changes from 2.63 to 0.79 compared to the data from the shell sample. It is suggested from the literature that the encapsulation of a nanoparticle inside a hollow spherical framework (e.g., virus capsid) could lead to the aforementioned changes.[49] Moreover, it is suggested (using the software Crysol) that these SAXS data of the core and shell samples fit quite well with the corresponding cluster structure models extracted from single-crystal X-ray diffraction, confirming the molecular structures and stability of core and shell structures.[50] More SAXS measurements were performed to study the two-week aged core−shell sample, which shows no obvious changes of the scattering curve when compared to that of a freshly prepared sample. This is strong evidence for the long-term stability of core−shell structure in aqueous solutions.

Extensive model fitting on the scattering curves is used to accurately locate the position of the core inside the shell structure. It is suggested from the single crystal structure that the core is right at the center of the shell because of their compatible sizes and symmetry.[42−45] However, due to the orientational disorder of the core unit and the complexation of gigantic molecular structures, the determination of accurate core position is difficult.[42−45] Moreover, the studies of core location in solutions could help understand the core−shell interaction and cluster-solvent interaction. In the crystal information files (CIFs) of the core−shell sample, only a small fraction of the atoms of the core can be located, mainly because of the enormous disorder of the core structures, which limits the application of Crysol in the fitting process.[42−45] Therefore, the building of artificial core−shell models from the existing core and shell structures is utilized here to fit the SAXS data. The location of the core inside the shell is determined through the following trial and error procedure. The core is first moved away from the center of the shell with a trial offset along a random direction. Then the scattering function is calculated from this newly built configuration following the standard approach detailed in previous literature, and in the experimental section.[28] The error is determined by $\chi^2 = \sum_i\{[I_{Mes}(q_i) - I_{th}(q_i)]/I_{Mes}(q_i)\}^2$, where I_{Mes} denotes the measured scattering data, I_{th} the theoretical scattering function calculated from a trial configuration, and q_i the scattering vector. The summation runs over all the data points from scattering measurements. The smaller the error is, the closer the constructed model is to the real molecules. We note that nine random directions are sampled for each trial offset and they yield quantitatively similar results suggesting the core and shell are isotropic objects in the studied length-scale. Two theoretical scattering functions with offsets of 0 and 2 Å comparing with the measurement is shown in Figure 3 and the χ^2 as a function of offsets is shown in the inset. It is clear that the configuration where the core and the shell are concentric best fits the experimental result, which is consistent with the assumptions in previous single crystal structure.[42−45]

The driving force for such a centering and stabilizing effect is found to be due to the presence of confined water molecules filling the space between the core and shell, as well as the existence of acetate groups. Structural analysis indicates that the dimension of acetate groups is appropriate to bridge the core and the shell gap. It is assumed that 16 acetate groups distribute homogeneously around the inner surface of the shell because of the high symmetry of crystals and clusters, which helps center the core structures. Moreover, QENS measurements of the core−shell sample without crystalline water at T = 300 K have been carried out; the data are presented in Figure 4. A Lorentzian function, with a full width at half-maximum (fwhm) of Γ = 54 μeV, is fitted to describe the quasi-elastic broadening of the data. Because of the large incoherent neutron scattering

DOI: 10.1021/jacs.5b11465
J. Am. Chem. Soc. 2016, 138, 2638−2643

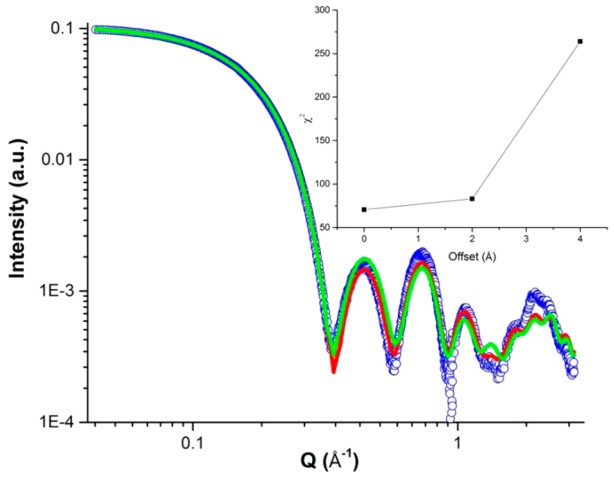

Figure 3. Simulated curves of core−shell models with core at the center (red) and 2 Å offset from the center (green) and the experimental SAXS data of the solution of core−shell samples (blue circle); Inset, the calculated χ^2 from the fitting of models with core offset various distances from the center. The simulation details can be found in the experimental section.

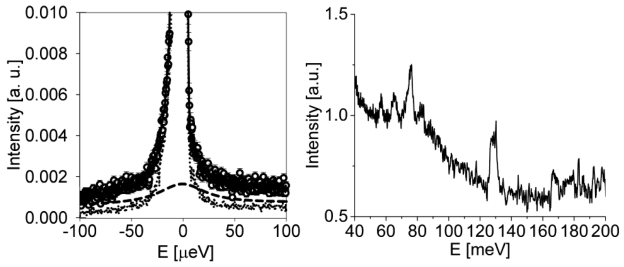

Figure 4. (a) QENS results averaged for 0.2 Å^{-1} < Q < 1.2 Å^{-1} (left) on the core−shell without crystalline water (circle, experimental data of the sample; dot, instrument resolution; dash line, the Lorentzian used for data fitting; solid line, the fitting data after combining instrument resolution and Lorentzian) and (b) INS results at 10 K (right) of the baked core−shell samples.

cross-section of hydrogen compared to other elements, the quasi-elastic signal is predominantly sensitive to the diffusion dynamics of water molecules in the system. The results indicate the existence of water molecules with slower dynamics compared to bulk water, which is a typical feature of confined water molecules (Figure 4). On the other hand, nondiffusing structural water molecules would not give rise to a quasi-elastic signal, contributing instead only to the elastic peak, which is also prominently present in the data shown in Figure 4. INS studies on the dried core−shell sample baked at 100 °C for 24 h show individual sharp peaks, suggesting the existence of only discrete water molecules in the dried core−shell structure, since clustered water structures usually show smooth curves with broad peaks. We believe that the dried sample after baking lost most of its confined water observed in QENS, while some structural water molecules, which are quite stable, remain in the sample after the heating process (Figure 4). It is believed that the peaks at 57, 64, and 75 meV are from the three vibrational modes of water molecules, and the one at 127 meV is from the vibration of the coordinated acetic acid group based on the energy level difference of the vibration modes. The vibrational modes of water molecules strongly depend on the local environment. The sharp vibrational features that are observed here imply order water structures.[51] A possible explanation is that the structure water molecules are in a constrained state because of the coordination to the surface metal ion center and the confinement in the space between the core and the shell. The neutron scattering studies suggest that there are two types of water molecules confined between the core and shell, which are responsible for centering of core structures and stabilizing the core−shell structures (see TOC).

Time-resolved SAXS studies of the synthetic reactions are able to detect the formation of the core−shell structure. The determination of the formation period of the shell structures is a critical question in the synthesis of gigantic POMs, which, however, has remained unresolved in previous publications describing the synthesis process. SAXS measurements of the synthetic reaction of the core−shell POM at different reaction stages suggest that the shell starts to form in solution 2.5 h after

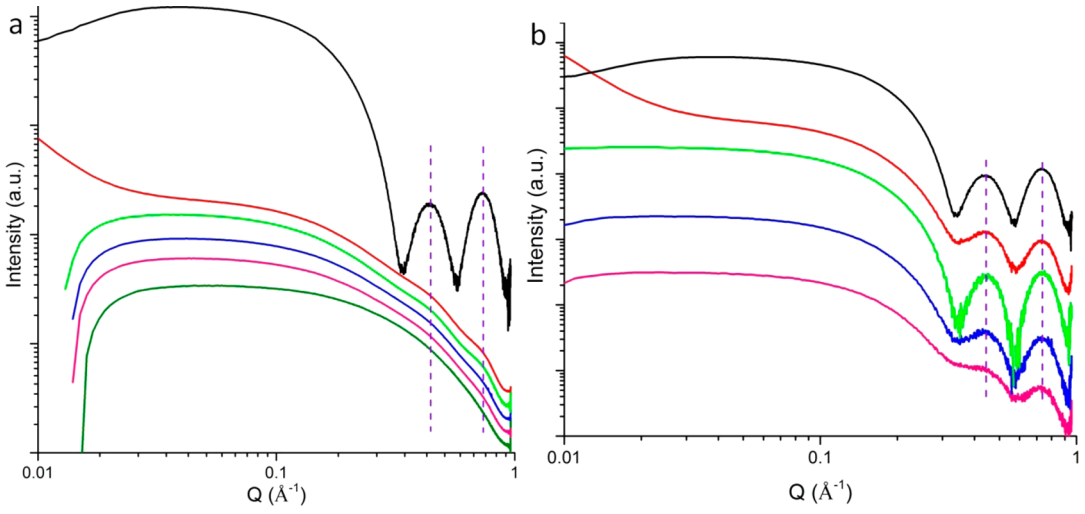

Figure 5. (a) Time-resolved SAXS monitoring of the synthetic reactions of core−shell POM with reaction time at 0 (olive), 2.5 (pink), 5 (blue), 19 (green), and 22 (red) h. As a standard for the scattering feature, the black curve is listed as experimental data of the solutions prepared from the crystals of core−shell structures: (b) the SAXS data at different reaction times (2.5, 5, 19, and 22 h) after subtracting the data at 0 h. The color code is the same as that of (a).

DOI: 10.1021/jacs.5b11465
J. Am. Chem. Soc. 2016, 138, 2638−2643

the reaction starts, not during the crystallization process, as witnessed by the appearance of the two oscillation peaks (blue curve in Figure 5a). Clearer results can be obtained by setting the data at 0 h as background and subtracting it from the other monitoring results (Figure 5b). The two peaks become more resolved as the reaction proceeds from 5 to 22 h. More information can be obtained qualitatively from the structure factor part at low Q range (0.01 to 0.1 $Å^{-1}$) of the data (Figure 5a). It is suggested from the previous literature that the upturn in structure factor is evidence for attraction, while the downturn is a sign of repulsion for the interaction among particles in solutions.[52] The structure factor of the curves suggests that a repulsive interaction exists in the reaction solution from 0 to 19 h, which means that the clusters in those solutions prefer to stay away from each other. However, an attractive interaction is observed in the reaction solution at 22 h, indicating that the formed core−shell clusters like to coagulate with each other. On the basis of the analysis above, the entire synthetic reaction can be described as follows: (1) Initiation: in the first 0−2.5 h, shell structure starts to form around the Keggin core; (2) Accumulation: from 2.5 to 19 h, the concentration of core−shell clusters increases; (3) Crystallization: after 22 h, the concentration of formed core−shell clusters reaches a critical value, and the clusters start coagulating and crystallizing. Meanwhile, SAXS monitoring results of the reaction without the adding of Keggin POM suggest that no shell structures were observed within 24 h (see Figure S1 in Supporting Information). It was also suggested in the existing literature that the synthetic reaction without Keggin POMs can produce the shell POMs only with a low yield and long reaction time (up to 3 weeks). It is believed that the Keggin POM might serve as the template for the growth of shell structures, which shortens the reaction time and enhances the yields of the final products.

CONCLUSION

The combination of X-ray and neutron scattering studies resolves three issues in the formation mechanism of the core−shell structures: (1) the core−shell structure is stable in solution with the core right at the center of the shell; (2) the core−shell structure starts to form in reaction solution within 5 h, not in the crystallization process; (3) there are water molecules confined in the space between the core and shell structures, which play vital roles in this templated synthetic reaction. Understanding the formation of presently known clusters is helpful in the design and synthesis of novel clusters and tuning of the physical and chemical properties of the clusters. The protocol we developed by using X-ray and neutron scattering techniques provides a convenient way to study *in situ* the reaction solutions of large clusters with high resolutions and short time intervals. This will be a general method in future research to fully explore the formation mechanism of different types of gigantic POMs.

ASSOCIATED CONTENT

Supporting Information

The Supporting Information is available free of charge on the ACS Publications website at DOI: 10.1021/jacs.5b11465.

Control SAXS experiment, synthesis of the core−shell POM, sample preparation for neutron scattering (PDF)

AUTHOR INFORMATION

Corresponding Author

*E-mail: yinp@ornl.gov

Notes

The authors declare no competing financial interest.

ACKNOWLEDGMENTS

P.Y. is grateful to the support of Clifford G. Shull Fellowship from Neutron Sciences Directorate of Oak Ridge National Laboratory. The research performed in BL-2 (BASIS) and BL-16B (VISION) at ORNL's Spallation Neutron Source was sponsored by the Scientific User Facilities Division, Office of Basic Energy Sciences, US Department of Energy. The sample preparation and initial SAXS study in the X-ray lab were conducted at the Center for Nanophase Materials Sciences, which is a DOE Office of Science User Facility. Oak Ridge National Laboratory is supported by the Office of Science of the US Department of Energy under Contract No. DE-AC05-00OR22725. The synchrotron-based SAXS study carried out in 12-ID-B and 12-ID-C used resources of the Advanced Photon Source, a U.S. Department of Energy (DOE) Office of Science User Facility operated for the DOE Office of Science by Argonne National Laboratory under Contract No. DE-AC02-06CH11357.

REFERENCES

(1) Müller, A.; Gouzerh, P. *Chem. Soc. Rev.* **2012**, *41*, 7431.
(2) Müller, A.; Kögerler, P.; Dress, A. W. M. *Coord. Chem. Rev.* **2001**, *222*, 193.
(3) Müller, A.; Peters, F.; Pope, M. T.; Gatteschi, D. *Chem. Rev.* **1998**, *98*, 239.
(4) Müller, A.; Kögerler, P. *Coord. Chem. Rev.* **1999**, *182*, 3.
(5) Kopilevich, S.; Müller, A.; Weinstock, I. A. *J. Am. Chem. Soc.* **2015**, *137*, 12740.
(6) Garai, S.; Rubčić, M.; Bögge, H.; Haupt, E. T. K.; Gouzerh, P.; Müller, A. *Angew. Chem., Int. Ed.* **2015**, *54*, 5879.
(7) Garai, S.; Rubčić, M.; Bögge, H.; Gouzerh, P.; Müller, A. *Chem. - Eur. J.* **2015**, *21*, 4321.
(8) Zang, H.-Y.; Miras, H. N.; Long, D.-L.; Rausch, B.; Cronin, L. *Angew. Chem., Int. Ed.* **2013**, *52*, 6903.
(9) Xu, F.; Miras, H. N.; Scullion, R. A.; Long, D.-L.; Thiel, J.; Cronin, L. *Proc. Natl. Acad. Sci. U. S. A.* **2012**, *109*, 11609.
(10) de la Oliva, A. R.; Sans, V.; Miras, H. N.; Yan, J.; Zang, H.; Richmond, C. J.; Long, D.-L.; Cronin, L. *Angew. Chem., Int. Ed.* **2012**, *51*, 12759.
(11) Liu, T. *Langmuir* **2010**, *26*, 9202.
(12) Yin, P.; Zhang, Z.-M.; Lv, H.; Li, T.; Haso, F.; Hu, L.; Zhang, B.; Bacsa, J.; Wei, Y.; Gao, Y.; Hou, Y.; Li, Y.-G.; Hill, C. L.; Wang, E.-B.; Liu, T. *Nat. Commun.* **2015**, *6*, 6475.
(13) Yin, P.; Li, D.; Liu, T. *Chem. Soc. Rev.* **2012**, *41*, 7368.
(14) Jing, B.; Hutin, M.; Connor, E.; Cronin, L.; Zhu, Y. *Chem. Sci.* **2013**, *4*, 3818.
(15) Li, H.; Yang, Y.; Wang, Y.; Wang, C.; Li, W.; Wu, L. *Soft Matter* **2011**, *7*, 2668.
(16) Zhang, L.; Li, H.; Wu, L. *Soft Matter* **2014**, *10*, 6791.
(17) Kurth, D. G.; Lehmann, P.; Volkmer, D.; Muller, A.; Schwahn, D. *J. Chem. Soc., Dalton Trans.* **2000**, 3989.
(18) Volkmer, D.; Du Chesne, A.; Kurth, D. G.; Schnablegger, H.; Lehmann, P.; Koop, M. J.; Müller, A. *J. Am. Chem. Soc.* **2000**, *122*, 1995.
(19) Mahon, E.; Garai, S.; Müller, A.; Barboiu, M. *Adv. Mater.* **2015**, *27*, 5165.
(20) Kögerler, P.; Müller, A. In *Polyoxometalate Molecular Science*; Borrás-Almenar, J., Coronado, E., Müller, A., Pope, M., Eds.; Springer: Netherlands, 2003; Vol. *98*, p 297.

DOI: 10.1021/jacs.5b11465
J. Am. Chem. Soc. 2016, 138, 2638−2643

(21) Merca, A.; Haupt, E. T. K.; Mitra, T.; Bögge, H.; Rehder, D.; Müller, A. *Chem. - Eur. J.* **2007**, *13*, 7650.
(22) Müller, A.; Sousa, F. L.; Merca, A.; Bögge, H.; Miró, P.; Fernández, J. A.; Poblet, J. M.; Bo, C. *Angew. Chem., Int. Ed.* **2009**, *48*, 5934.
(23) Todea, A. M.; Merca, A.; Bögge, H.; Glaser, T.; Pigga, J. M.; Langston, M. L. K.; Liu, T.; Prozorov, R.; Luban, M.; Schröder, C.; Casey, W. H.; Müller, A. *Angew. Chem., Int. Ed.* **2010**, *49*, 514.
(24) Robbins, P. J.; Surman, A. J.; Thiel, J.; Long, D.-L.; Cronin, L. *Chem. Commun.* **2013**, *49*, 1909.
(25) Nakamura, I.; Miras, H. N.; Fujiwara, A.; Fujibayashi, M.; Song, Y.-F.; Cronin, L.; Tsunashima, R. *J. Am. Chem. Soc.* **2015**, *137*, 6524.
(26) Müller, A.; Shah, S. Q. N.; Bogge, H.; Schmidtmann, M. *Nature* **1999**, *397*, 48.
(27) Miras, H. N.; Cooper, G. J. T.; Long, D.-L.; Bögge, H.; Müller, A.; Streb, C.; Cronin, L. *Science* **2010**, *327*, 72.
(28) Zemb, T.; Lindner, P. *Neutrons, X-rays and Light: Scattering Methods Applied to Soft Condensed Matter*; Elsevier: New York, 2002.
(29) Sadeghi, O.; Zakharov, L. N.; Nyman, M. *Science* **2015**, *347*, 1359.
(30) Yin, P.; Li, T.; Forgan, R. S.; Lydon, C.; Zuo, X.; Zheng, Z. N.; Lee, B.; Long, D.; Cronin, L.; Liu, T. *J. Am. Chem. Soc.* **2013**, *135*, 13425.
(31) Hou, Y.; Zakharov, L. N.; Nyman, M. *J. Am. Chem. Soc.* **2013**, *135*, 16651.
(32) Yin, P.; Bayaguud, A.; Cheng, P.; Haso, F.; Hu, L.; Wang, J.; Vezenov, D.; Winans, R. E.; Hao, J.; Li, T.; Wei, Y.; Liu, T. *Chem. - Eur. J.* **2014**, *20*, 9589.
(33) Antonio, M. R.; Nyman, M.; Anderson, T. M. *Angew. Chem., Int. Ed.* **2009**, *48*, 6136.
(34) Kojima, T.; Antonio, M. R.; Ozeki, T. *J. Am. Chem. Soc.* **2011**, *133*, 7248.
(35) Pigga, J. M.; Kistler, M. L.; Shew, C.-Y.; Antonio, M. R.; Liu, T. *Angew. Chem., Int. Ed.* **2009**, *48*, 6538.
(36) Qiu, J.; Ling, J.; Sui, A.; Szymanowski, J. E. S.; Simonetti, A.; Burns, P. C. *J. Am. Chem. Soc.* **2012**, *134*, 1810.
(37) Liao, Z.; Deb, T.; Nyman, M. *Inorg. Chem.* **2014**, *53*, 10506.
(38) Qiu, J.; Nguyen, K.; Jouffret, L.; Szymanowski, J. E. S.; Burns, P. C. *Inorg. Chem.* **2013**, *52*, 337.
(39) Svergun, D.; Koch, M. H. J. *Rep. Prog. Phys.* **2003**, *66*, 1735.
(40) Putnam, C. D.; Hammel, M.; Hura, G. L.; Tainer, J. A. *Q. Rev. Biophys.* **2007**, *40*, 191.
(41) *Mater. Today* **2002**, *5*, 38. 10.1016/S1369-7021(02)01142-2
(42) Todea, A. M.; Al-Karawi, A. J. M.; Glaser, T.; Walleck, S.; Chamoreau, L.-M.; Thouvenot, R.; Gouzerh, P.; Müller, A. *Inorg. Chim. Acta* **2012**, *389*, 107.
(43) Muller, A.; Das, S. K.; Bogge, H.; Schmidtmann, M.; Botar, A.; Patrut, A. *Chem. Commun.* **2001**, 657.
(44) Müller, A.; Das, S. K.; Kögerler, P.; Bögge, H.; Schmidtmann, M.; Trautwein, A. X.; Schünemann, V.; Krickemeyer, E.; Preetz, W. *Angew. Chem., Int. Ed.* **2000**, *39*, 3413.
(45) Todea, A. M.; Szakács, J.; Konar, S.; Bögge, H.; Crans, D. C.; Glaser, T.; Rousselière, H.; Thouvenot, R.; Gouzerh, P.; Müller, A. *Chem. - Eur. J.* **2011**, *17*, 6635.
(46) Mamontov, E.; Herwig, K. W. *Rev. Sci. Instrum.* **2011**, *82*, 085109.
(47) Azuah, R. T.; Kneller, L. R.; Qiu, Y.; Tregenna-Piggott, P. L. W.; Brown, C. M.; Copley, J. R. D.; Dimeo, R. M. *J. Res. Natl. Inst. Stand. Technol.* **2009**, *114*, 341.
(48) Seeger, P. A.; Daemen, L. L.; Larese, J. Z. *Nucl. Instrum. Methods Phys. Res., Sect. A* **2009**, *604*, 719.
(49) Li, T.; Chattopadhyay, S.; Shibata, T.; Cook, R. E.; Miller, J. T.; Suthiwangcharoen, N.; Lee, S.; Winans, R. E.; Lee, B. *J. Mater. Chem.* **2012**, *22*, 14458.
(50) Svergun, D.; Barberato, C.; Koch, M. H. J. *J. Appl. Crystallogr.* **1995**, *28*, 768.
(51) Ockwig, N. W.; Cygan, R. T.; Hartl, M. A.; Daemen, L. L.; Nenoff, T. M. *J. Phys. Chem. C* **2008**, *112*, 13629.
(52) Qiu, X.; Kwok, L. W.; Park, H. Y.; Lamb, J. S.; Andresen, K.; Pollack, L. *Phys. Rev. Lett.* **2006**, *96*, 138101.

DOI: 10.1021/jacs.5b11465
J. Am. Chem. Soc. 2016, 138, 2638−2643